observation, and the phase plots of the secondary observations are consistent with that distribution in both phase and width. The χ^2 value for the light curve in Fig. 1 is 127 for 19 degrees of freedom, giving a formal probability of chance occurrence of less than 10^{-17}. The H-test[17], an unbinned statistical method, gives a value of 98, which indicates that the formal probability (O. C. DeJager, personal communication) of this being a random distribution is 10^{-17}. Below 500 MeV, the pulsed radiation is harder to recognize above the diffuse galactic radiation, and no pulsed emission is visible below 100 MeV. No statistically significant time structure is seen within the envelope of the pulse, although the shape suggests two wide pulses separated by 0.2 in phase. This pulse shape is markedly different from those of the Crab, Vela and Geminga γ-ray pulsars, all of which show two narrow peaks with a separation of 0.4–0.5 period. Figure 1 also shows the arrival time of the radio pulse, which occurs 0.22 ± 0.02 phase before the leading edge of the γ-ray pulse. This is a larger offset than seen for Vela, where the radio pulse leads the peak of the first γ-ray pulse by 0.126 ± 0.006 phase[19].

Figure 2 shows a preliminary energy spectrum of the pulsed γ-radiation above 100 MeV, based on the primary observation in July 1991. Pulsed emission is seen to at least 5,000 MeV. The spectrum during this fraction 0.35 of the pulse period can be fitted with a power law

$$dN/dE_\gamma = (8.93 \pm 0.76) \times 10^{-10} (E_\gamma/622.4)^{-1.72 \pm 0.08}$$
$$\text{photons cm}^{-2}\,\text{s}^{-1}\,\text{MeV}^{-1} \quad (1)$$

with E_γ in MeV.

The energy scale factor, 622.4 MeV, is chosen so that the statistical errors in the power law index and the overall normalization are uncorrelated. This spectrum is considerably flatter than the pulsed spectrum seen from the Crab (ref. 19; and P.L.N. *et al.*, manuscript in preparation), which has a spectral index ≤ -2.0. The pulsed emission from Vela, although time-variable, has been seen to have a flat spectrum similar to that of PSR1706 − 44 during some observations (ref. 20; and G.K. *et al.*, manuscript in preparation).

The time-averaged spectrum has the same form as equation (1), but with a normalization of $(3.12 \pm 0.27) \times 10^{-10}$. The time-averaged flux of PSR1706 − 44 above 100 MeV is $(1.0 \pm 0.3) \times 10^{-6}$ photons cm^{-2} s^{-1}, where the quoted uncertainty includes both the statistics and an uncertainty from the spectral fitting. Between 100 and 5,000 MeV, the energy flux is $(8.2 \pm 2.5) \times 10^{-10}$ erg cm^{-2} s^{-1}. For a distance of 1.5 kpc and beaming into 3.4 steradian (an assumed value based on the pulse width), this represents 6.1×10^{34} erg s^{-1} or about 1.8% of the spin-down energy loss of 3.4×10^{36} erg s^{-1}, comparable to that seen in the Vela pulsar for similar assumptions[20]. Except for the shape of the light curve, therefore, the observed features of PSR1706 − 44 strongly resemble those of the Vela pulsar.

Gamma-ray emission from fast pulsars can be interpreted as radiation (curvature radiation, inverse Compton scattering or synchrotron radiation) from particles accelerated in the pulsar magnetosphere, either near the surface[21] or in vacuum gaps in the outer magnetosphere[22]. The broad pulse seen for PSR1706 − 44 implies that the geometry of the spin axis and magnetic axis relative to the direction of the observer differs from that for the Crab, Vela or Geminga. Future observations may reveal timing structure within the PSR1706 − 44 pulse which will clarify the geometry. The phase diagram does not preclude the possibility of a double-pulse structure with a narrower separation than those seen for the Crab and Vela γ-ray pulsars. □

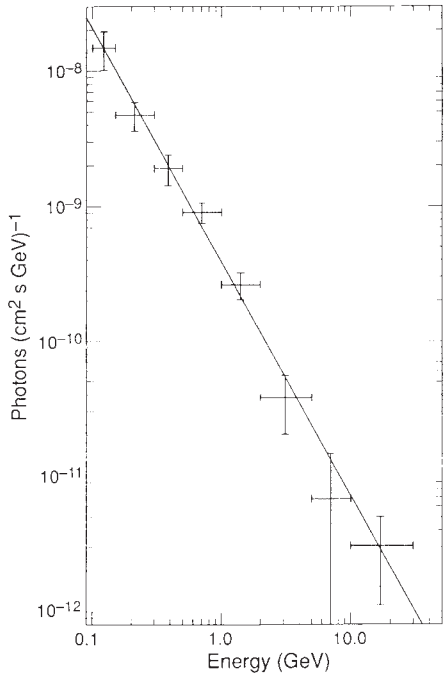

FIG. 2 Energy spectrum of PSR1706 − 44 during the pulsed phase (0.55–0.90 from Fig. 1). The error bars shown are statistical only.

Received 27 May; accepted 17 August 1992.

1. Thompson, D. J., Fichtel, C. E., Hartman, R. C., Kniffen, D. A. & Lamb, R. C. *Astrophys. J.* **213,** 252–262 (1977).
2. Kanbach, G. *et al. Astr. Astrophys.* **90,** 163–169 (1980).
3. Ögelman, H. B., Fichtel, C. E., Kniffen, D. A. & Thompson, D. J. *Astrophys. J.* **209,** 584–591 (1976).
4. Thompson, D. J., Bertsch, D. L., Hartman, R. C. & Hunter, S. D. *Astr. Astrophys.* **127,** 220–223 (1983).
5. Buccheri, R. *et al. Astr. Astrophys.* **128,** 245–251 (1983).
6. Harding, A. K. *Astrophys. J.* **245,** 267–273 (1981).
7. Ruderman, M. & Cheng, K. S. *Astrophys. J.* **335,** 306–318 (1988).
8. Wilson, R. B. *et al. IAU Circ.* No. 5429 (1992).
9. Halpern, J. P. & Holt, S. S. *Nature* **357,** 222–224 (1992).
10. Bertsch, D. L. *et al. Nature* **357,** 306–307 (1992).
11. Hughes, E. B. *et al. IEEE Trans. Nucl. Sci.* **NS-27,** 364–369 (1980).
12. Kanbach, G. *et al. Space Sci. Rev.* **49,** 69–84 (1988).
13. Kanbach, G. *Gamma Ray Obs. Sci. Workshop Proc.*, 2-1-2-10 (1989).
14. Swanenburg, B. N. *et al. Astrophys. J.* **243,** L69–L73 (1981).
15. Johnston, S. *et al. Mon. Not. R. astr. Soc.* **255,** 401–411 (1992).
16. Thompson, D. J. *et al. Astrophys. J. Suppl.* (in the press).
17. DeJager, O. C., Swanepoel, J. W. H. & Raubenheimer, B. C. *Astr. Astrophys.* **221,** 180–190 (1978).
18. Buccheri, R. *et al. Astr. Astrophys.* **69,** 141–142 (1978).
19. Clear, J. *et al. Astr. Astrophys.* **174,** 85–94 (1987).
20. Grenier, I. A., Hermsen, W. & Clear, J. *Astr. Astrophys.* **204,** 117–132 (1988).
21. Daugherty, J. K. & Harding, A. *Astrophys. J.* **252,** 337–347 (1982).
22. Cheng, K. S., Ho, C. & Ruderman, M. *Astrophys. J.* **300,** 500–521 (1986).

Pulsar glitches as probes of neutron star interiors

Bennett Link, Richard I. Epstein & Kenneth A. Van Riper

Los Alamos National Laboratory, Los Alamos, New Mexico 87545, USA

PULSAR rotation rates generally decrease steadily owing to external electromagnetic braking torques, but occasionally show sudden increases ('glitches') followed by gradual recoveries that may last days or years. These events are thought to be consequences of angular momentum transfer between a solid crust, which rotates at the measured pulsar periodicity, and a more rapidly rotating 'loose' component of the neutron star interior. Sudden braking of the differential rotation between the two components will cause a glitch[1], and the subsequent re-establishment of rotational equilibrium between the two components represents the recovery[2]. Earlier studies, using particular models for the coupling between crust and interior, showed that the loose component carries ~2.8% and ≳1% of the total moment of inertia of the Vela pulsar[3] and PSR 1737 − 30 (ref. 4) respectively. Here, we analyse post-glitch recovery in four pulsars, and deduce that the loose component

carries at least 0.8% of the total moment of inertia, independent of the form of the coupling. In the context of the 'vortex creep' model of recovery, in which the loose component is the inner-crust neutron superfluid[2,5–7], the constraint on the moment of inertia rules out equations of state that are soft at high densities.

Typical pulsar spin behaviour across a glitch is illustrated in Fig. 1. In the absence of glitches or other violent changes, the decelerations of the crust $\dot{\Omega}_c(t) \equiv d\Omega_c(t)/dt$ and the loose component both approach an asymptotic rate $\dot{\Omega}_\infty(t)$. In principle, the loose component can rotate differentially, in which case its angular velocity $\Omega_l(t, \mathbf{r})$ is a function of position. The loose component slows because of drag by the crust, and hence $\Omega_l(t, \mathbf{r}) \geq \Omega_c(t)$. When there is no glitch activity, all of the loose component slows and transfers angular momentum to the crust, so $\dot{\Omega}_l(t, \mathbf{r}) \leq 0$ and $\dot{J}_l \equiv \int \dot{\Omega}_l(t, \mathbf{r})\, dI_l \leq 0$, where J_l is the angular momentum of the loose component and I_l its moment of inertia. During a glitch at time t_g (see Fig. 1), the crust increases its angular velocity by an amount $\Delta\Omega_c$, and then decelerates more rapidly than before the glitch. After time t_r, the recovery time, the crust's rotation rate falls below its value before the glitch: $\Omega_c(>t_r) < \Omega_c(<t_g)$. When $t_g < t < t_r$, the crust spins faster than before the glitch, and possibly spins faster than some of the loose component. During this interval, the crust may impart angular momentum to the loose component. After t_r, however, the crust must once again have a lower angular velocity than all of the loose component so that its angular momentum is decreasing: $\dot{J}_l(>t_r) < 0$.

We define $I \equiv I_c + I_l$ to be the total effective moment of inertia of the star, where I_c is the moment of inertia of the solid crust plus any parts of the star tightly coupled to it. From angular momentum conservation,

$$I_c\dot{\Omega}_c(t) + \dot{J}_l(t) = N_{ext} \quad (1)$$

where the external torque is $N_{ext} \equiv -I|\dot{\Omega}_\infty(t)|$. Because $\dot{J}_l < 0$ for $t > t_r$ (but before the next glitch) we have

$$I_c|\dot{\Omega}_c(>t_r)| \leq I|\dot{\Omega}_\infty(>t_r)| \quad (2)$$

Although $\dot{\Omega}_\infty(t)$ is not directly observable, it can be compared to the crust spin-down rate. We first note that the external torque decreases as the pulsar evolves so that $|\dot{\Omega}_\infty(>t_r)| < |\dot{\Omega}_\infty(<t_g)|$, although the difference is extremely small. Second, because $\Omega_c(t)$ approaches $\Omega_\infty(t)$ before the glitch, we have $|\dot{\Omega}_\infty(<t_g)| < |\dot{\Omega}_c(<t_g)|$, as can be seen from Fig. 1. With these two inequalities and $I_c = I - I_l$, equation (2) becomes $(I - I_l)|\dot{\Omega}_c(>t_r)| < I|\dot{\Omega}_c(<t_g)|$, and hence

$$\frac{I_l}{I} > 1 - \frac{\dot{\Omega}_c(>t_r)}{\dot{\Omega}_c(<t_g)} \quad (3)$$

A lower limit on I_l can be obtained for any time after t_r and before the next glitch, but the strongest constraint is obtained for times close to t_r, when $|\dot{\Omega}_c|$ is still relatively large. The lower limit on I_l/I derived from equation (3) is less than the fractional change in $\dot{\Omega}_c$ across the glitch, as some of the discontinuity in the spin-down rate decays by t_r.

To account for uncertainties in glitch times, we use the following procedure. We extrapolate the fit of $\Omega_c(t)$ for the pre-glitch data to the time of the first post-glitch measurement at time t'_g; we denote this quantity by $\Omega_{ex}(t'_g)$ (see Fig. 1). The corresponding recovery time, t'_r, is found from $\Omega_c(t'_r) = \Omega_{ex}(t'_g)$. Because t'_r always exceeds t_r, we use $\dot{\Omega}_c(t'_r)$ for $\dot{\Omega}_c(>t_r)$ in equation (3). For the quantity $\dot{\Omega}_c(<t_g)$ we evaluate $\dot{\Omega}_c(t)$ at the time of the last pre-glitch observation. In practice $\dot{\Omega}_c(<t_g)$ varies so slowly that the precise time used is unimportant.

Table 1 shows lower limits on I_l/I obtained from data on selected glitches in PSRs 0531+21 (Crab), 0833−45 (Vela), 0355+54 and 0525+21. We also tabulate the approximate glitch date (which is $\leq t'_g$), the discontinuities in Ω_c and $\dot{\Omega}_c$ across each glitch (indicated with the subscript g), and the interval $t'_r - t'_g$. In the cases of the Crab pulsar and PSR0525+21, recovery occurs so soon after the glitch (as reflected in the small values for $t'_r - t'_g$) that little of the initial discontinuity in $\dot{\Omega}_c$ decays, and the limit on I_l is $I_l/I \geq (\Delta\dot{\Omega}_c/\dot{\Omega}_c)_g$. In the Vela pulsar, on the other hand, much of the discontinuity in $\dot{\Omega}_c$ decays before t'_r. The 1975 giant glitch of the Vela pulsar yields the most stringent constraint on the moment of inertia of the loose component: $I_l/I \geq 0.0081$.

What is the loose component likely to be? The most promising candidate is the neutron superfluid in the inner crust. This region, where nuclei coexist with a free neutron gas, extends from the density of neutron drip 4.3×10^{11} g cm^{-3}, to the density of nuclear matter, $\rho_0 = 2.8 \times 10^{14}$ g cm^{-3}. The angular velocity of a superfluid is determined by the spatial arrangement of its vortex lines. In regions of the inner crust, vortex interactions with nuclei inhibit vortex motion so that the superfluid responds only slowly to changes in the angular velocity of the crust[2,5–7], and the coupling between this portion of the superfluid and the crust is weak. By contrast, in the core, where superfluid neutrons co-exist with superconducting protons, entrainment of protons by the flowing neutrons induces magnetic moments about the vortices. Electron scattering from magnetized vortices causes the core superfluid to achieve corotation with the crust within minutes after a glitch[8]. Over timescales typical of post-glitch response, therefore, the solid crust and core behave essentially as a single rigid body.

Hereafter we assume that the loose component is the inner-crust superfluid, and write $I_s \equiv I_l$. In principle, the loosely coupled component could comprise all of the free neutrons of the inner crust. Within current theoretical uncertainties, inner-crust superfluidity may extend up to nuclear density[9] ρ_0, or may cease to exist above densities as low as $\sim 0.27\ \rho_0$ (ref. 10). To allow for the possibility that only a fraction of the free neutrons of the inner crust contributes to I_s, we treat the maximum density to which superfluidity extends as a parameter ρ_{max}.

In general, for a given mass, stellar models with softer equations of state have thinner inner crusts with smaller moments of inertia. In Fig. 2, we show the fractional moment of inertia of the crustal superfluid as a function of neutron star mass for selected maximum densities for superfluidity ($\rho_{max}/\rho_0 = 1.0$, 0.7 and 0.5) and the following equations of state: BPS (Reid soft-core nucleon potential and hyperons[11]), P (Reid potential and pure neutron matter[12]), FP (two- and three-nucleon interactions[12]), BJ (Reid potential with short-range repulsion and hyperons[14]), CCLR (two-body Levinger–Simmons potential[15]) and PS (nucleon coupling to a mean scalar field[16]).

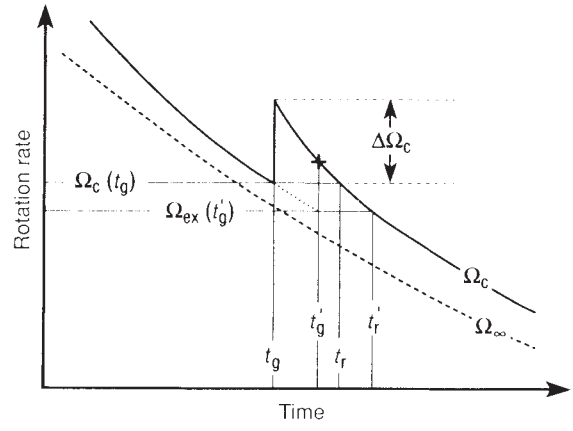

FIG. 1 Schematic evolution of the crust angular velocity Ω_c through a glitch. After a glitch at time t_g, the pulsar recovers its pre-glitch rotation rate at t_r. The first post-glitch measurements (shown by the +) are at t'_g and the corresponding recovery time is t'_r. The dashed line represents the asymptotic spin rate Ω_∞.

TABLE 1 Glitch parameters

PSR	$\Omega/2\dot{\Omega}$ (yr)	Date (month/yr)	Ref.	$10^8(\Delta\Omega/\Omega)_g$	$10^2(\Delta\dot{\Omega}/\dot{\Omega})_g$	$t'_r - t'_g$ (day)	$10^2 I_i/I >$
0531+21 (Crab)	1.2 K	2/75	21	3.8	0.25	0.04	0.25
		8/86	22	0.92	0.25	0.008	0.23
0833−45 (Vela)	11 K	2/69	23	234	1.0	19	0.63*
		8/71	23	205	1.5	17	0.72
		9/75	23	199	1.1	16	0.81
		7/78	23	306	1.8	25	0.70
		10/81	23	114	0.84	9	0.67
			24	115	4.9	9	0.70
		8/82	23	205	2.3	17	0.65
			24	206	6.3	17	0.74
		7/85	24	160	1.4	13	0.68
		12/88	25	181	7.7	15	0.76
0355+54	0.6 M	1/85	26	0.56	0.18	2.3	0.16
0525+21	1.5 M	1/74	27	0.13	0.46	1.4	0.37

* In using the fitting formulae of ref. 23, we used the pre-glitch $\dot{\Omega}_c$ extrapolated to t'_g.

Observations suggest that neutron star masses are close to 1.4 solar masses ($M_\odot$). For example, the masses of PSR1913+16 and its companion (also believed to be a neutron star) are $1.442 \pm 0.003\ M_\odot$ and $1.386 \pm 0.003\ M_\odot$, respectively[17]. The BPS equation of state is inconsistent with these observations as it supports a maximum stable mass of only $1.414\ M_\odot$, which is ~2% lower than the measured mass of PSR1913+16.

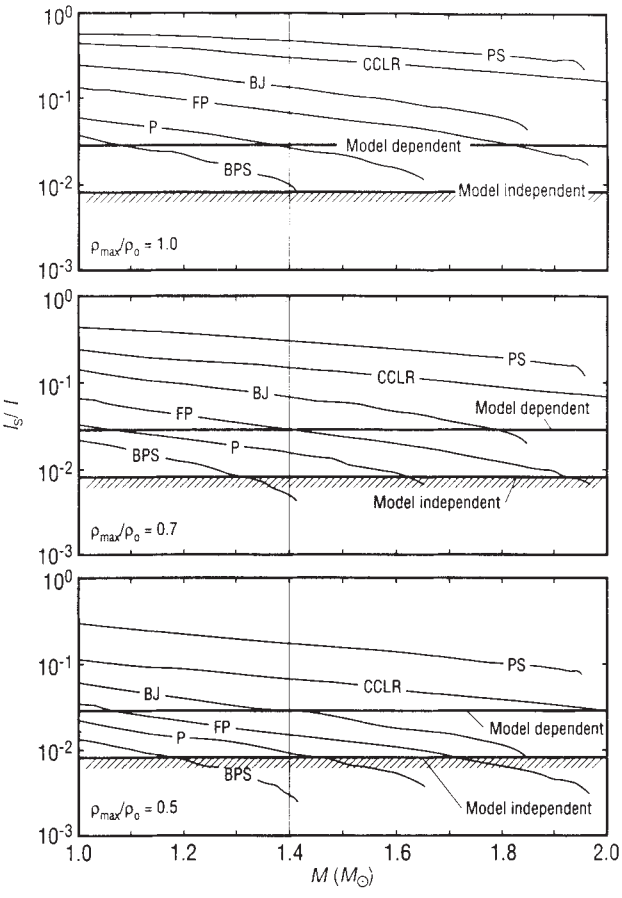

FIG. 2 Fractional moment of inertia of the inner crust superfluid as a function of neutron star mass for selected equations of state and maximum densities ρ_{max} for superfluidity. The model-independent constraint obtained here and the model-dependent estimate obtained in ref. 3 are shown. Values of I_s that fall in the cross-hatched regions are ruled out.

In Fig. 2 our lower limit $I_s/I \geq 0.0081$ is shown. The model-dependent estimate[3] of $I_s/I \approx 0.028$ is shown for comparison. We see that for $\rho_{max}/\rho_0 = 1.0$, the model-independent constraint on I_s is barely consistent with the Vela pulsar being a $1.4\ M_\odot$ neutron star with a soft equation of state (such as BPS), and the model-dependent estimate excludes this possibility. For the more plausible case of $\rho_{max}/\rho_0 = 0.7$, soft equations of state are ruled out for any reasonable mass of the Vela pulsar, whereas a moderately stiff equation of state (such as FP) is consistent with the model-dependent estimate. For superfluidity extending to $0.5\ \rho_0$, moderately stiff equations of state are allowed by the model-independent constraint, although not by the model-dependent estimate (BPS, P and FP all excluded).

More recent equations of state are stiffer than BPS and P, and yield maximum neutron star masses of 1.8–2.2 $M_\odot$ (see for example, ref. 18). Brown[19] has argued, however, that the equation of state may be much softer than generally thought, and suggests that the maximum stable neutron star mass is near $1.5\ M_\odot$. Brown *et al.*[20] propose that the failure to observe a pulsar in supernova 1987A indicates that the core collapsed to form a black hole, as would be the case if the equation of state were very soft. The theoretical situation is far from resolved, but the method presented here, when applied to future timing data, may help settle this issue. □

Received 3 April; accepted 7 August 1992.

1. Anderson, P. W. & Itoh, N. *Nature* **256,** 25–27 (1975).
2. Alpar, M. A., Anderson, P. W., Pines, D. & Shaham, J. *Astrophys. J.* **276,** 325–334 (1984).
3. Pines, D. & Alpar, M. A. in *Structure and Evolution of Neutron Stars* (eds Pines, D., Tamagaki, R. & Tsuruta, S.) (New York, Addison-Wesley, in the press).
4. Michel, F. C., Bland Hawthorn, J. & Lyne, A. G. *Mon. Not. R. astr. Soc.* **246,** 624–627 (1990).
5. Link, B. & Epstein, R. I. *Astrophys. J.* **373,** 592–603 (1991).
6. Link, B., Epstein, R. I. & Baym, G. *Astrophys. J.* (in the press).
7. Epstein, R. I. & Baym, G. *Astrophys. J.* **328,** 680–690 (1988).
8. Alpar, M. A., Langer, S. A. & Sauls, J. A. *Astrophys. J.* **282,** 533–541 (1985).
9. Ainsworth, T. L., Wambach, J. & Pines, D. *Phys. Lett.* B**222,** 173–178 (1989).
10. Chen, J. M. C., Clark, J. W., Krotscheck, E. & Smith, R. A. *Nucl. Phys.* A**451,** 509–540 (1986).
11. Baym, G., Pethick, C. & Sutherland, P. *Astrophys. J.* **170,** 299–317 (1971).
12. Pandharipande, V. R. *Nucl. Phys.* A**174,** 641–656 (1971).
13. Friedman, B. & Pandharipande, V. R. *Nucl. Phys.* A**361,** 502–520 (1981).
14. Bethe, H. A. & Johnson M. *Nucl. Phys.* A**230,** 1–58 (1976).
15. Cohen, J. M., Langer, W. D., Rosen, L. C. & Cameron, A. G. W. *Astrophys. Space Sci.* **6,** 228–239 (1970).
16. Pandharipande, V. R. & Smith, R. A. *Phys. Lett.* B**59,** 15–18 (1975).
17. Wolszczan, A. *Nature* **350,** 688–690 (1991).
18. Wiringa, R. B., Fiks, V. & Fabrocini, A. *Phys. Rev.* C**38,** 1010–1037 (1988).
19. Brown, G. E. *Nature* **336,** 519–520 (1988).
20. Brown, G. E., Bruenn, S. W. & Wheeler, J. C. *Comments Astrophys.* (in the press).
21. Lohsen, E. H. G. *Astr. Astrophys. Suppl.* **44,** 1–14 (1981).
22. Lyne, A. G. & Pritchard, R. S. *Mon. Not. R. astr. Soc.* **229,** 223–226 (1987).
23. Cordes, J. M., Downs, G. S. & Krause-Polstorff, J. *Astrophys. J.* **330,** 847–869 (1988).
24. McCulloch, P. M., Klekociuk, A. R., Hamilton, P. A. & Royle, G. W. R. *Aust. J. Phys.* **40,** 725–730 (1987).
25. McCulloch, P. M., Hamilton, P. A., McConnell, D. & King, E. A. *Nature* **346,** 822–824 (1990).
26. Lyne, A. G. *Nature* **326,** 569–571 (1987).
27. Downs, G. S. *Astrophys. J.* **257,** L67–L70 (1982).

ACKNOWLEDGEMENTS. This work was carried out under the auspices of the U.S. Department of Energy.